Tracer Kinetic Modeling of ^{11}C-Acetate Applied in the Liver With Positron Emission Tomography

Sirong Chen*, Chilai Ho, Dagan Feng, *Fellow, IEEE*, and Zheru Chi, *Member, IEEE*

***Abstract*—It is well known that 40%–50% of hepatocellular carcinoma (HCC) do not show increased ^{18}F-fluorodeoxyglucose (FDG) uptake. Recent research studies have demonstrated that ^{11}C-acetate may be a complementary tracer to FDG in positron emission tomography (PET) imaging of HCC in the liver. Quantitative dynamic modeling is, therefore, conducted to evaluate the kinetic characteristics of this tracer in HCC and nontumor liver tissue. A three-compartment model consisting of four parameters with dual inputs is proposed and compared with that of five parameters. Twelve regions of dynamic datasets of the liver extracted from six patients are used to test the models. Estimation of the adequacy of these models is based on Akaike Information Criteria (AIC) and Schwarz Criteria (SC) by statistical study. The forward clearance $\mathrm{K} = \mathrm{K_1} * \mathrm{k_3}/(\mathrm{k_2} + \mathrm{k_3})$ is estimated and defined as a new parameter called the local hepatic metabolic rate-constant of acetate (LHMRAct) using both the weighted nonlinear least squares (NLS) and the linear Patlak methods. Preliminary results show that the LHMRAct of the HCC is significantly higher than that of the nontumor liver tissue. These model parameters provide quantitative evidence and understanding on the kinetic basis of ^{11}C-acetate for its potential role in the imaging of HCC using PET.**

***Index Terms*—local hepatic metabolic rate-constant of acetate (LHMRAct), modeling, parameter estimation, positron emission tomography (PET), ^{11}C-acetate.**

I. Introduction

THE hallmark of positron emission tomography (PET) is its ability to quantify *in vivo* the physiological and biochemical processes in humans using intravascularly injected PET tracers. Kinetic modeling using ^{18}F-fluorodeoxyglucose (FDG) is well established for measurements of many physiological parameters, but little attention has been given to the quantitative evaluation of liver metabolism, in spite of its central role as the "power house" of the human body. The use of PET for the studying of liver disease has been mostly in the detection of liver tumors [1]. Hepatocellular carcinoma (HCC) is the seventh most common malignancy worldwide in men and the ninth in women. Its occurrence is much higher in the Asian and African. It is one of the top three causes of cancer death in many Asian localities including China, Taiwan, Singapore and Japan. The disease is also believed to be in an upward trend in America due to the increasing frequency of hepatitis C viral infection [2] and it is also a common cause of cancer deaths among Asian immigrants. Most cases of HCC are discovered late and less than 10% are cured with surgical resection. Overall 5-year survival rate is less than 5% [3], [4].

The rate of glucose metabolism (glycolysis) is increased in many forms of malignant tumors. It is directly correlated with tumor proliferation. The investigation of tumor kinetics by FDG-PET imaging has recently suggested that HCC has a nonzero dephosphorylation kinetic constant $\mathrm{k_4}$ [5]. A nonzero $\mathrm{k_4}$ is due to the presence of the enzyme glucose-6-phosphatase in HCC, the abundance of which leads to leakage of the trapped FDG metabolite back to the circulation. This may account for one of the reasons that 40%–50% of HCC are not FDG-avid. This is regarded as the Achilles' heel of FDG-PET in the evaluation of liver tumors and is clearly not acceptable in countries where this tumor is one of the top three causes of cancer deaths.

Recently, we have investigated the usefulness of ^{11}C-acetate in imaging HCC and other liver masses. Preliminary research findings have suggested that this agent might have a great potential role as a complementary tracer to and perhaps a better tracer than FDG [6], [7]. Fig. 1 demonstrates a case of recurrent HCC in the left lobe of liver after right lobectomy. CT shows hypervascularity within the tumor. FDG-PET imaging shows no abnormal FDG uptake by the tumor, whereas ^{11}C-acetate PET imaging shows increased metabolism.

^{11}C-acetate is a common tracer for the investigation of regional myocardial oxidative metabolism [8], [9]. However, no data exist in the literature regarding the investigation of ^{11}C-acetate on HCC. The exact metabolic pathway of ^{11}C-acetate within tumors such as HCC is not well understood, although participation through acetyl-CoA in Beta oxidation for free fatty acid synthesis is thought to be the preferred biochemical method of incorporation. Application of kinetic modeling techniques may in addition provide improved understanding of these complex biokinetic processes [10]. In this research, a three-compartment four-parameter (4-P) kinetic model with dual inputs for evaluation of ^{11}C-acetate metabolism in liver is proposed. Comparison of this 4-P model and a three-compartment five-parameter (5-P) model with dual inputs is conducted.

Manuscript received July 12, 2002; revised November 12, 2003. This work was supported by the studentship of the Hong Kong Polytechnic University, in part by RGC (PolyU5134/99E) and ARC grants. The Associate Editor responsible for coordinating the review of this paper and recommending its publication was M. A. Viergever. *Asterisk indicates corresponding author.*

*S. Chen is with the Center for Multimedia Signal Processing, Department of Electronic and Information Engineering, The Hong Kong Polytechnic University, Kowloon, Hong Kong (e-mail: ensrchen@eie.polyu.edu.hk).

C. Ho is with the Department of Nuclear Medicine & PET, Hong Kong Sanatorium & Hospital, Happy Valley, Hong Kong (e-mail: garrettho@hksh.com).

D. Feng is with the Center for Multimedia Signal Processing, Department of Electronic and Information Engineering, The Hong Kong Polytechnic University, Kowloon, Hong Kong, and the Biomedical & Multimedia Information Technology Group, School of Information Technologies, The University of Sydney, Sydney, 2006 Australia (e-mail: enfeng@polyu.edu.hk).

Z. Chi is with the Center for Multimedia Signal Processing, Department of Electronic and Information Engineering, The Hong Kong Polytechnic University, Kowloon, Hong Kong (e-mail: enzheru@polyu.edu.hk).

Digital Object Identifier 10.1109/TMI.2004.824229

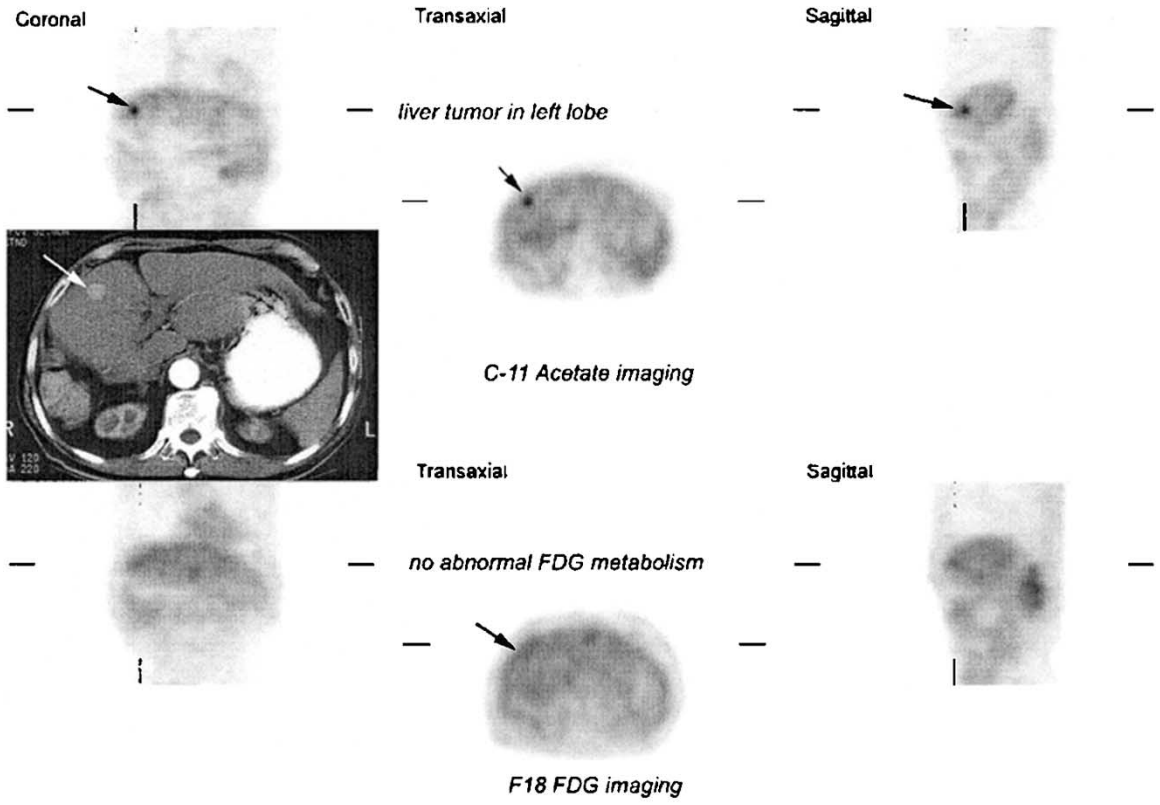

Fig. 1. CT demonstrates a hypervascular lesion in the L lobe of liver (status post R lobectomy for HCC); FDG imaging shows no abnormal FDG uptake; ^{11}C-acetate imaging shows increased metabolism.

A new physiological parameter called "local hepatic metabolic rate-constant of acetate (LHMRAct)" is introduced to characterize the regional consumption of acetate by both tumor and nontumor tissue of the liver.

II. Methods

A. PET Scanning

An ECAT-EXACT 47 PET scanner (CTI/Siemens, Inc., TN) is used for transaxial (septa-extended) dynamic image acquisition. Full sets of dynamic data in one single position, covering the liver dome and apical half of the left ventricle (LV) to the inferior part of liver, are obtained for 10 min immediately following bolus IV injection of ^{11}C-acetate. Sampling acquisition sequence is as follows: 4-s frames $\times$ 10, 10-s frames $\times$ 8, 30-s frames $\times$ 2; 60-s frames $\times$ 3 and 120-s frames $\times$ 2, a total of 25 frames. Standard static PET imaging covering the entire liver is also performed from 10–20 min. Then FDG is injected and FDG-PET imaging is performed 1 h later (allowing more than 4 half-life decay for ^{11}C-acetate).

B. Human Studies

Six patients, all are hepatitis B carriers, including two with HCC, were recruited into the study. Twelve regions of dynamic datasets, two from HCC regions, were extracted.

C. Blood Time-Activity Dual Input Functions

The tracer time-activity curve in blood (BTAC) $c_b(t)$ is used as the input function in the kinetic model. BTAC is usually represented by a sequence of arterial or arterialized blood samples. However, blood sampling is in general very invasive and requires extra personnel and processing time. Several noninvasive techniques have been proposed. One is proposed to extract the input function together with the physiological parameters from the brain dynamic images [11]. Chen, *et al.* [12] has reported using the TAC obtained from the region of interest (ROI) drawn on the target organ during dynamic PET imaging as an input function. The utilization of image-derived input function has been more commonly used in quantitative PET studies of the heart [13]. The reliability of using BTAC obtained directly by drawing a ROI over the LV or the left arterial region are investigated in [14]. Double modeling approach for dynamic cardiac studies with PET to estimate physiological parameter is also proposed [15].

The liver has a dual source of blood supply, receiving oxygenated blood from the common left and right hepatic arteries (HAs) and nutrient-rich blood via the portal vein (PV) [16]. Therefore, the use of arterial input may, however, introduce systematic errors in the estimated kinetic parameters because of the ignorance of the hepatic dual blood supply from the HA and the PV to the liver [1]. It is highly invasive and virtually impossible in clinical settings to count the radioactivity of the portal venous blood by direct catheterization and sampling. For the modeling method, the existence of dual blood supply in the liver would necessitate twice the number of parameters required for full characterization. For preliminary investigation, this method of modeling appears impractical. Therefore, image-derived BTAC appears to be the only option at the moment.

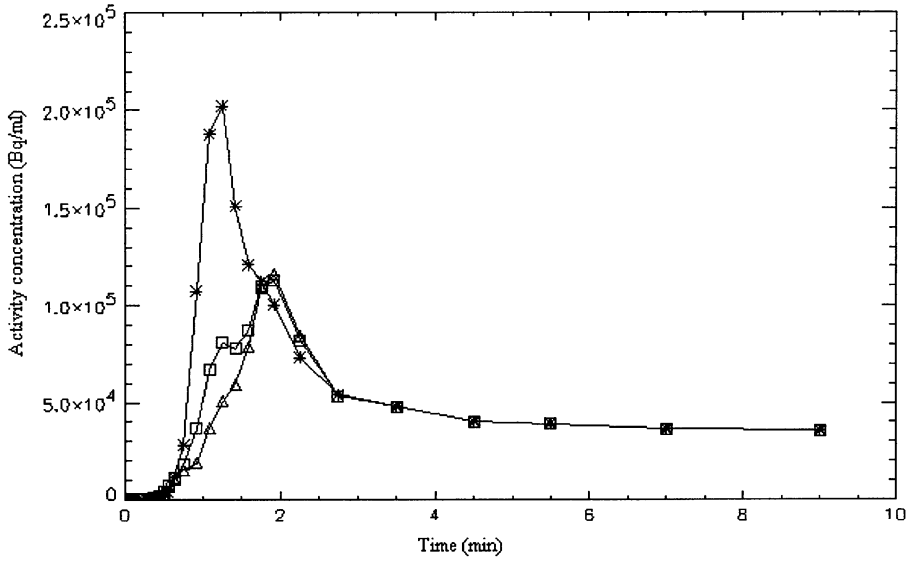

Fig. 2. Typical HA, PV and weighted dual-input function of the nontumor tissue. Solid line marked by asterisk stands for HA, triangle for the PV and square for the weighted dual-input. The greatest activity difference among these 3 curves is during the initial radionuclide angiographic phase.

In this work, the BTAC is obtained directly from PET images measurements. To reduce the scattering effect of radioactivity from the adjacent tissue, the contribution from the HA is approximated by evaluating the activity-time curve of the abdominal aorta adjacent to the liver instead of the LV. The contribution from the PV is evaluated by direct activity-time measurement. The tracer arriving at the PV is delayed and dispersed when compared with that of the HA, making its activity similar to that of the tracer in the nontumor liver tissue. Therefore, it is difficult to differentiate the PV from the surrounding hepatic parenchyma. However, its location may still be identified by its invariable anatomical position being posterior to the pancreatic head that shows the most intense physiological uptake of ^{11}C-acetate, or by direct reference to the CT images. The radioactivity spillover from the surrounding tissue to the PV is significant, especially at the later part of the study when the tracer concentration in tissue is much higher than that in the PV. Munk *et al.* [1] suggested that the difference between the two blood TACs was most pronounced around the peak and immediately after the bolus injection. After some time they are virtually identical. Therefore, the last five measurements of the TACs of the PV from PET imaging are replaced by the HA data in this study. To strike a reasonable statistical balance without compromising physiological requirement, the BTAC is measured empirically by using fixed weights from these two blood supply inputs, viz. 20% contribution from HA and 80% from PV according to their approximate percentage perfusion to the nontumor liver tissue. Thus, the dual-input function is calculated according to

$$c_b(t) = c_a(t) * 20\% + c_v(t) * 80\% \tag{1}$$

where $c_a(t)$ is the tracer concentration in the HA and $c_v(t)$ is the tracer concentration in the PV. However, the majority of the blood supply to the tumor is from the HA rather than the PV, accordingly, the weights of tumor used in this paper is 80% contribution from HA and 20% from PV or 100% contribution from HA. Fig. 2 shows an example of typical blood TACs from the HA, the PV and the weighted dual-input function for the nontumor tissue.

In this preliminary study, the metabolites of ^{11}C-acetate in blood are not taken into consideration in order not to complicate the issue of defining the "suitable" model. Also no correction is made for the noise scatters of the inputs.

D. Liver Kinetic Model for ^{11}C-Acetate

It is not just a clinical observation that HCC may display variable tumor kinetics. Early research on rat hepatomas had suggested that the patterns of glycolytic enzymes might reflect hepatoma cell growth, function, and graded dedifferentiation [17]. Preliminary study shows that in some cases, FDG and ^{11}C-acetate are taken up by different parts of the tumor, suggesting that mixed pathology with dual tracer kinetics could exist within these tumors. Past researches on PET tracer kinetic modeling have been reported [18]–[20], but there is no data on kinetic modeling of ^{11}C-acetate PET imaging in the liver. Acetate is enzymatically converted into acetyl-CoA in the liver [21], and then enters the Kreb's Cycle. In the liver, the role of Kreb's Cycle is more complex than in heart muscles [21]. Although the exact biochemical mechanism of ^{11}C-acetate accumulation within HCC is not completely defined, there is evidence that acetate is channeled to acetyl-CoA for fatty acid (lipid) synthesis in tumor cells, instead of being metabolized to CO_2 through the Kreb's cycle [22]. It is, therefore, reasonable to assume that only one compartment is needed for all of the metabolites in the liver/tumor tissue. A three-compartment model, as shown in Fig. 3, is proposed in this study. The left compartment of this model represents the intravascular ^{11}C-acetate concentration. The center compartment represents the intracellular ^{11}C-acetate concentration. The right compartment represents the intracellular products/metabolites converted from ^{11}C-acetate (acetyl-CoA, and metabolites of fatty acid synthesis). K_1 represents the first order rate constant for the transport of ^{11}C-acetate from blood to tissue, k_2 for reverse transport of ^{11}C-acetate from tissue to blood, k_3 for conversion

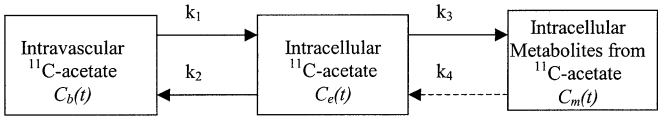

Fig. 3. Three-compartment liver kinetic model for ^{11}C-acetate.

of ^{11}C-acetate to its products/metabolites, and k_4 for back conversion from the products/metabolites to ^{11}C-acetate. It should be noted that although the real biological system is complex, this compartmental approach, nonetheless, represents a rather reasonable estimation for global physiological function [10]. Since the number of compartments of this proposed ^{11}C-acetate liver model is the same as that of the FDG model originally proposed by Sokoloff *et al.* [18] and further extended by Huang *et al.* [19] and Phelps *et al.* [20], the differential equations to the ^{11}C-acetate liver 5-P model share the same form as the FDG model

$$\frac{d}{dt}c_e(t) = K_1 c_b(t) - (k_2 + k_3)c_e(t) + k_4 c_m(t) \quad (2)$$

$$\frac{d}{dt}c_m(t) = k_3 c_e(t) - k_4 c_m(t) \quad (3)$$

$$c_i(t) = c_e(t) + c_m(t) \quad (4)$$

where $c_b(t)$ is the ^{11}C-acetate concentration in whole blood, $c_e(t)$ is the free ^{11}C-acetate concentration in intracellular space, $c_m(t)$ is the intracellular products/metabolites concentration, and $c_i(t)$ is the sum of $c_e(t)$ and $c_m(t)$. The solution of $c_i(t)$ in terms of macroparameters is

$$c_i(t) = (B_1 e^{-L_1 t} + B_2 e^{-L_2 t}) \otimes c_b(t) \quad (5)$$

where

$$B_1 = \frac{K_1}{\alpha_2 - \alpha_1}(k_3 + k_4 - \alpha_1), \quad L_1 = \alpha_1$$

$$B_2 = \frac{K_1}{\alpha_2 - \alpha_1}(\alpha_2 - k_3 - k_4), \quad L_2 = \alpha_2$$

$$\alpha_{1,2} = \frac{k_2 + k_3 + k_4 \mp \sqrt{(k_2 + k_3 + k_4)^2 - 4k_2k_4}}{2}.$$

B_1, B_2, L_1, and L_2 are the macroparameters in the model [11] and $\otimes$ denotes the operation of temporal convolution. If k_4 approaches zero, for simplicity, letting k_4 be zero, thus the macroparameters of the 4-P model are given by

$$B_1 = \frac{K_1 k_3}{k_2 + k_3}, \quad L_1 = 0$$

$$B_2 = \frac{K_1 k_2}{k_2 + k_3}, \quad L_2 = k_2 + k_3. \quad (6)$$

Regions of interest (ROIs) are drawn at 75% threshold of maximal pixel count around the margin of the liver tumor automatically by the supplied scanner software. The same ROI is used to measure the activity of nontumor liver tissue. TACs are thus generated.

The total activity of tracer in tissue includes both the activity of hepatic parenchyma and the activity within vascular/sinus space of liver tissue. As the blood volume in the liver is fairly large, a hepatic blood volume (HBV) term is included in our proposed ^{11}C-acetate model to account for this effect. The observed total tissue activity $c_T(t)$, is

$$c_T(t) = c_i(t) + \mathrm{HBV} * c_b(t). \quad (7)$$

With the measurements of both BTAC $c_b(t)$ and TTAC $c_T(t)$, the rate constants K_1 to k_4 and HBV are estimated by the weighted nonlinear least square (NLS) methods.

E. Statistical Study

The weighted NLS algorithms are used to numerically evaluate all the individual parameters. Statistical analysis, including standard deviation (SD) and coefficient of variation (CV), is performed. The CV of a parameter estimate is calculated from

$$\mathrm{CV}_P = \frac{\mathrm{SD}_P}{P} \times 100\% \quad (8)$$

where P is the parameter estimate and SD_P is the SD of P [11]. Model parameters are estimated by minimizing the weighted residual sum of squares (WRSS) [1]. In our research, the weights are proportional to the frame duration divided by the concentration value of that time point. We assume that the data variances are known up to a constant. Three-compartment 4-P and 5-P models are used to fit the clinical data. The best model fitted to the data is not necessarily the model producing the smallest WRSS, because adding more parameters generally decreases the WRSS [1]. The Akaike Information Criteria (AIC) [23] and Schwarz Criteria (SC) [24] are used to test which one is the best. The AIC and the SC are given by (in the case that the data variances are known up to a constant)

$$\mathrm{AIC} = N \ln(\mathrm{WRSS}) + 2P \quad (9)$$

$$\mathrm{SC} = N \ln(\mathrm{WRSS}) + P \ln N \quad (10)$$

where P is the number of parameters in the model, and N is the number of data points. The best model by the AIC or SC is the one that minimizes the AIC or SC, respectively. The AIC or SC provides a balance between data fitting precision in the first term and minimum dimensionality in the second [23], [24].

F. Model Estimation of the LHMRAct

The newly proposed physiological parameter LHMRAct is calculated using the following formula:

$$\mathrm{LHMRAct} = \frac{K_1 k_3}{k_2 + k_3} \quad (11)$$

where K_1 to k_3 can be derived from the results of NLS fitting. When k_4 is assumed to be zero, Patlak analysis [25] can also be applied to this study. The ratio of $c_T(t)$ and $c_b(t)$ can be calculated by

$$\frac{c_T(t)}{c_b(t)} = \frac{K}{c_b(t)} \int_0^t c_b(\tau)d\tau + \frac{K_1 k_2}{(k_2 + k_3)^2} + \mathrm{HBV} \quad (12)$$

where

$$K = \frac{K_1 k_3}{k_2 + k_3}.$$

The data points within the period 2.5–10 min are chosen to estimate the LHMRAct using Patlak method. The fitting results are compared with those obtained from the NLS methods by correlation analysis.

III. Results and Conclusion

Both the weighted NLS algorithms and the linear Patlak analysis are used. The ^{11}C-acetate clinical data from twelve

TABLE I
RESULTS OF THE THREE-COMPARTMENT 4-P MODEL WITH DUAL INPUTS FOR LIVER USING ^{11}C-ACETATE

Datasets number	Rate constants				Criterion	
	K_1 (ml/min/ml)	k_2 (min^{-1})	k_3 (min^{-1})	HBV (ml/ml)	AIC	SC
1	0.666±0.045	0.241±0.054	0.056±0.041	0.036±0.024	194.1	198.9
2	0.651±0.044	0.306±0.055	0.090±0.030	0.039±0.020	180.3	185.1
3	0.726±0.057	0.277±0.060	0.060±0.035	0.048±0.027	197.1	202.0
4	0.760±0.033	0.292±0.032	0.052±0.016	0.035±0.015	164.0	168.9
5	0.457±0.017	0.237±0.027	0.075±0.020	0.383±0.013	144.2	149.1
6	0.459±0.040	0.243±0.057	0.071±0.035	0.367±0.023	173.5	178.4
7	0.651±0.054	0.424±0.071	0.151±0.023	0.367±0.027	162.6	167.5
8	0.685±0.096	0.500±0.126	0.160±0.031	0.395±0.043	183.7	188.6
9*	1.118±0.054	0.309±0.040	0.107±0.020	0.090±0.023	187.9	192.8
10	0.907±0.058	0.230±0.042	0.043±0.027	0.162±0.029	177.7	182.5
11	0.648±0.059	0.349±0.077	0.124±0.035	0.034±0.024	169.6	174.5
12*	0.638±0.058	0.243±0.155	0.705±0.248	0.073±0.016	167.0	171.9

* Regions 9 and 12 represent HCC. The input function of region 9 is totally from the TAC of HA. The dual input functions of region 12 is: 80% contribution from HA and 20% from PV.

TABLE II
RESULTS OF THE THREE-COMPARTMENT 5-P MODEL WITH DUAL INPUTS FOR LIVER USING ^{11}C-ACETATE

Datasets number	Rate constants					Criterion	
	K_1 (ml/min/ml)	k_2 (min^{-1})	k_3 (min^{-1})	k_4 (min^{-1})	HBV (ml/ml)	AIC	SC
1	0.651±0.188	0.227±0.166	0.053±0.211	0.038±0.882	0.038±0.026	195.4	201.5
2	0.656±0.244	0.332±0.286	0.117±0.043	0.012±0.162	0.037±0.023	184.2	190.3
3	0.717±0.273	0.271±0.106	0.064±0.117	0.025±0.413	0.050±0.030	198.6	204.7
4	0.759±0.097	0.298±0.069	0.071±0.182	0.086±0.536	0.035±0.018	165.1	171.2
5	0.450±0.144	0.228±0.071	0.072±0.053	0.014±0.217	0.385±0.013	146.3	152.4
6	0.440±0.487	0.218±0.384	0.059±0.135	0.011±0.287	0.377±0.026	173.8	179.8
7	0.669±0.222	0.456±0.309	0.175±0.042	0.021±0.069	0.360±0.032	164.4	170.5
8	0.703±0.172	0.536±0.290	0.177±0.155	0.014±0.125	0.389±0.051	185.0	191.1
9*	1.134±0.122	0.328±0.086	0.132±0.115	0.034±0.143	0.085±0.025	189.5	195.6
10	0.928±0.165	0.234±0.105	0.050±0.258	0.074±1.046	0.150±0.033	178.5	184.6
11	0.653±0.177	0.358±0.287	0.146±.0.124	0.037±0.191	0.032±0.029	171.5	177.6
12*	0.640±1.715	0.255±0.957	0.761±0.392	0.010±0.020	0.069±0.020	168.7	174.8

* Regions 9 and 12 represent HCC. The input function of region 9 is totally from the TAC of HA. The dual input functions of region 12 is: 80% contribution from HA and 20% from PV.

ROIs are analyzed to test the 4-P and 5-P models and several statistical criteria are used to validate their adequacy. Results are given as the estimated value $\pm$ SD. The parameter estimations by the weighted NLS algorithms are summarized in Tables I and II. The model fitted curves according to the 4-P and 5-P models for two randomly chosen datasets are shown in Fig. 4. As seen in Tables I and II, the estimated values of the parameters for the two models are quite close to each other, but the CVs of the estimated parameters for the 4-P model are far smaller than those for the 5-P model. For the 5-P model, the CVs of the estimated K_1 range from 10.7% to 38.0% except region 6 (where CV of $\mathrm{K}_1 = 111\%$) and region 12 (where CV of $\mathrm{K}_1 = 268\%$). The CVs of the estimated k_2 range from 23.2% to 86.2% except region 6 (where CV of $\mathrm{k}_2 = 176\%$) and region 12 (where CV of $\mathrm{k}_2 = 374\%$). Only 7 CVs of the estimated k_3 among the 12 sets of data are under 100% and the CVs of the estimated k_4 are far from acceptable. The CVs of the estimated HBV vary greatly according to the estimated values themselves. For the HBV whose estimated values are under or around 0.05, the CVs vary from 51.3% to 92.8%. For the other HBV values, the CVs range from 3.4% to 29.7%. Since the estimated k_4 values are very small and are less reliable for interpretation, it is reasonable to assume k_4 to be zero during the first 10-min dynamic scan. For the 4-P model, the CVs of the estimated K_1 are all less than 10% except region 8 (where CV of $\mathrm{K}_1 = 14.0\%$). The CVs of the estimated k_2 range from 10.9% to 25.2% except region 12 (where CV of $\mathrm{K}_2 = 64.0\%$). The CVs of the estimated k_3 range from 15.4% to 72.6%. The CVs of the estimated HBV values show no significant difference from those estimated by the 5-P model. For those estimated values under or around 0.05, the CVs range from 42.9% to 70.0%. For the remaining ROIs', the CVs range from 3.3% to 25.2%. Since the vascularity of cirrhotic liver is heterogeneous, the estimated HBV values also exhibit moderate variability. The 4-P model is statistically better than the 5-P model. Though the values of the WRSS for the 4-P model are slightly larger than those for the 5-P model, the CVs, the AICs and SCs for the 4-P model are all less than those of the 5-P model, suggesting that the 4-P model is the best model to characterize the kinetics of ^{11}C-acetate in the liver. Moreover, the fitting results of the 4-P model are less affected by the initial values whereas those of 5-P model were greatly affected. Table III shows the results of the estimated LHMRAct by the NLS and the linear Patlak methods. The correlation coefficients between the results of Patlak method and those of the 4-P model and the 5-P model using the NLS method are 97.2% and 94.9%, respectively. The results are not very ideal; perhaps this is due to certain simplification already discussed

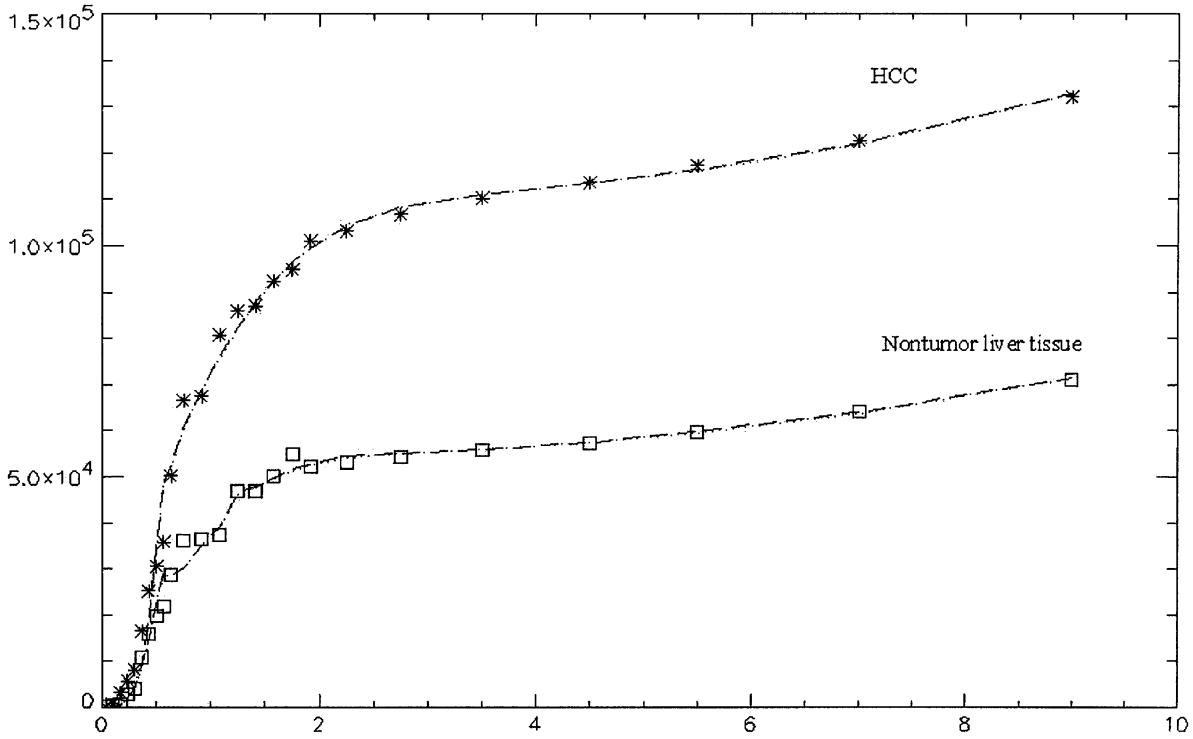

Fig. 4. Graph shows the generated TACs of the HCC ROI and the nontumor liver tissue ROI with symbol $*$. While, dashed lines are the results of the fitted TACs using 5-P model; dotted lines are the results of the fitted TACs using 4-P model.

TABLE III
RESULTS OF ESTIMATION OF THE LHMRAct FOR THE 4-P AND 5-P MODELS WITH DUAL INPUTS USING THE NLS AND PATLAK METHODS

Datasets number	Estimated LHMRAct (K_1*k_3/(k_2+k_3))		
	NLS method using the 5-P model	NLS method using the 4-P model	Patlak method
1	0.1235	0.1263	0.1809
2	0.1708	0.1472	0.1684
3	0.1366	0.1292	0.1826
4	0.1466	0.1142	0.1548
5	0.1080	0.1095	0.1562
6	0.0934	0.1040	0.1494
7	0.1854	0.1705	0.1611
8	0.1747	0.1666	0.1601
9*	0.3249	0.2883	0.2644
10	0.1614	0.1436	0.1836
11	0.1894	0.1695	0.1869
12*	0.4790	0.4743	0.4682

* Regions 9 and 12 represent HCC. The input function of region 9 is totally from the TAC of HA. The dual input functions of region 12 is: 80% contribution from HA and 20% from PV.

before. Other limitations include a moderate amount of noise scatters intrinsically found in all dynamic PET sampling protocols, as well as a high degree of freedom (21), potentially leading to fitting difficulties. From compartment analysis using the NLS algorithms for 4-P model, the following physiological parameters are obtained. For nontumor liver tissue, the mean value of $\mathrm{K_1}$ is 0.661 ml/min/ml; $\mathrm{k_2}$ is 0.310/min; $\mathrm{k_3}$ is 0.088 /min. The estimated forward clearance K (LHMRAct) by the NLS and Patlak methods are 0.1381 ± 0.0252 ml/min/ml and 0.1684 ± 0.0139 ml/min/ml, respectively. For the two ROIs of HCC, the estimated LHMRAct by the NLS methods are 0.2883 ml/min/ml and 0.4743 ml/min/ml and by the Patlak method are 0.2644 ml/min/ml and 0.4682 ml/min/ml, respectively. The LHMRAct of the non-FDG-avid type of HCC (regions 9 and 12) are significantly higher than those of the nontumor liver parenchyma ($p < 0.05$). Although among the twelve datasets there are only two suffering from HCC, the functional parameters of ^{11}C-acetate in this tumor have shown statistically significant difference. Therefore, parametric imaging with ^{11}C-acetate metabolism measured quantitatively (LHMRAct) may add supportive evidence of the usefulness of this tracer to tumor detection.

In summary, this three-compartment 4-P model with dual input functions has been found suitable in mapping the kinetic characters of ^{11}C-acetate in a 10-min dynamic PET imaging of the liver. The model has provided a better understanding of the complexity and biochemistry of the behavior of this tracer in HCC and nontumor liver tissue. A 10-min dynamic

acquisition of ^{11}C-acetate PET imaging may provide enough valuable quantitative data. These findings suggest that the LHMRAct could be considered as potential indicators of metabolism (other than SUV) for evaluating HCC. ^{11}C-acetate is a complementary tracer and perhaps a better tracer than FDG for detection of HCC.

REFERENCES

[1] O. L. Munk, L. Bass, K. Roelsgaard, D. Bender, S. B. Hansen, and S. Keiding, "Liver kinetics of glucose analogs measured in pigs by PET: Importance of dual-input blood sampling," *J. Nucl. Med.*, vol. 42, no. 5, pp. 795–801, 2001.

[2] H. El-Serag, "Epidemiology of hepatocellular carcinoma," *Clin. Liver Dis.*, vol. 5, pp. 87–107, 2001.

[3] T. Tsuzuki, A. Sugioka, and M. Ueda, "Hepatic resection for hepatocellular carcinoma," *Surgery*, vol. 107, pp. 511–520, 1990.

[4] K. T. Watkins and S. A. Curley, "Liver and bile ducts," in *Clinical Oncology*, 2nd ed, M. D. Abeloff, J. O. Armitage, A. S. Lichter, and J. E. Niederhuber, Eds. New York: Churchill Livingstone, 2000, pp. 1681–1748.

[5] S. Okazumi, K. Isono, K. Enomoto, T. Kikuchi, M. Ozaki, H. Yamamoto, H. Hayashi, T. Asano, and M. Ryu, "Evaluation of liver tumors using fluorine-18-fluorodeoxyglucose PET: Characterization of tumor and assessment of effect of treatment," *J. Nucl. Med.*, vol. 33, no. 3, pp. 333–339, 1992.

[6] C.-L. Ho, S. Yu, and D. Yeung, "^{11}C-acetate PET imaging in hepatocellular carcinoma and other liver masses," *J. Nucl. Med.*, vol. 44, no. 2, pp. 213–221, 2003.

[7] D. Delbeke and C. Pinson, "^{11}C-acetate: A new tracer for the evaluation of hepatocellular carcinoma," *J. Nucl. Med.*, vol. 44, no. 2, pp. 222–223, 2003.

[8] A. Buck, H. G. Wolpers, G. D. Hutchins, V. Savas, T. J. Managner, N. Nguyen, and M. Schwaiger, "Effect of carbon-11-acetate recirculation on estimates of myocardial oxygen consumption by PET," *J. Nucl. Med.*, vol. 32, no. 10, pp. 1950–1957, 1991.

[9] K. T. Sun, K. Chen, S. C. Huang, D. B. Buxton, H. W. Hansen, A. S. Kim, S. Siegel, Y. Choi, P. Muller, M. E. Phelps, and H. R. Schelbert, "Compartment model for measuring myocardial oxygen consumption using [1-^{11}C] acetate," *J. Nucl. Med.*, vol. 38, no. 3, pp. 459–466, 1997.

[10] D. Feng, S. C. Huang, and X. Wang, "Models for computer simulation studies of input functions for tracer kinetic modeling with positron emission tomography," *Int. J. Biomed. Computing*, vol. 32, pp. 95–110, 1993.

[11] D. Feng, K. P. Wong, C. M. Wu, and W. C. Siu, "A technique for extracting physiological parameters and the required input function simultaneously from PET image measurements: Theory and simulation study," *IEEE Trans. Inform. Technol. Biomed.*, vol. 1, pp. 243–254, Jan. 1997.

[12] K. Chen, D. Bandy, E. Reiman, S. C. Huang, M. Lawson, D. Feng, L. Yun, and A. Palant, "Noninvasive quantification of the cerebral metabolic rate for glucose using positron emission tomography, ^{18}F-fluoro-2-deoxyglucose, the patlak method, and an image-derived input function," *J. Cereb. Blood Flow Metab.*, vol. 18, pp. 716–723, 1998.

[13] R. R. Raylman, J. M. Caraher, and G. D. Hutchins, "Sampling requirements for dynamic cardiac PET studies using image-derived input functions," *J. Nucl. Med.*, vol. 34, no. 3, pp. 440–447, 1993.

[14] X. Li, D. Feng, K. Lin, and S. C. Huang, "Estimation of myocardial glucose utilization with PET using the left ventricular time-activity curve as a noninvasive input function," *Med. Biol. Eng. Computing*, vol. 36, no. 1, pp. 112–117, 1998.

[15] D. Feng, X. Li, and S. C. Huang, "A new double modeling approach for dynamic cardiac PET studies using noise and spillover contaminated LV measurements," *IEEE Trans. Biomed. Eng.*, vol. 43, pp. 319–327, Mar. 1996.

[16] L. P. Dartner and J. L. Hiatt, *Color Textbook of Histology*, Philadelphia: Saunders, 1997.

[17] C. E. Shonk, H. P. Morris, and G. E. Boxer, "Patterns of glycolytic enzymes in rat liver and hepatoma," *Cancer Res.*, vol. 25, pp. 671–676, 1965.

[18] L. Sokoloff, M. Reivich, C. Kennedy, M. H. Des Rosiers, C. S. Patlak, K. D. Pettigrew, O. Sakurada, and M. Shinohara, "The [^{14}C] Deoxyglucose method for the measurement of local cerebral glucose utilization: Theory, procedure, and normal values in the conscious and anesthetized albino rat," *J. Neurochem.*, vol. 28, pp. 897–916, 1977.

[19] S. C. Huang, M. E. Phelps, E. J. Hoffman, K. Sideris, C. J. Selin, and D. E. Kuhl, "Noninvasive determination of local cerebral metabolic rate of glucose in man," *Amer. J. Physiol.*, vol. 238, pp. E69–E82, 1980.

[20] M. E. Phelps, S. C. Huang, E. J. Hoffman, C. Selin, L. Sokoloff, and D. E. Kuhl, "Tomographic measurement of local cerebral glucose metabolic rate in humans with (F-18)2-Fluoro-2-Deoxy-D-Glucose: Validation of method," *Ann. Neurol.*, vol. 6, pp. 371–388, 1979.

[21] L. Stryer, *Biochemistry*, 4th ed. New York: Freeman, 1995, pt. III, ch. 20.

[22] M. Yoshimoto *et al.*, "Characterization of acetate metabolism in tumor cells in relation to cell proliferation: Acetate metabolism in tumor cells," *Nucl. Med. Biol.*, vol. 28, pp. 117–122, 2001.

[23] H. Akaike, "A new look at the statistical model identification," *IEEE Trans. Automat. Contr.*, vol. AC-19, pp. 716–723, 1974.

[24] G. Schwarz, "Estimating the dimension of a model," *Ann. Statist.*, vol. 6, pp. 461–564, 1978.

[25] C. S. Patlak, R. G. Blasberg, and J. D. Fenstermacher, "Graphical evaluation of blood-to-brain transfer constants from multiple-time uptake data," *J. Cereb. Blood Flow Metab.*, vol. 3, pp. 1–7, 1983.